Sliding Mode Sensorless Control of Induction Motor Using Variable Frequency Models

Amuliu Bogdan Proca, *Ph. D Student*
Ali Keyhani, *Professor*

Abstract: A sensorless torque control system for induction motors was developed in this research. The system allows for fast and precise torque tracking over a wide range of speed. Unlike most research in the area, the authors used an induction motor model that adapts its parameters to the operating conditions. An adaptive sliding mode observer is developed for speed observation and a cascade of discrete time sliding mode controllers is used for flux and current control. A least-square estimation speed estimation method is used at very low speed (below 20 rpm). Simulation and experimental results prove the validity of the approach.

Index Terms: Sensorless control, adaptive, sliding mode, modeling, parameter estimation, induction motor

Nomenclature

v_{ds}, v_{qs} : stator voltage in stationary reference frame

i_{ds}, i_{qs} : currents in stationary reference frame

i_{ds}^e, i_{qs}^e : currents in synchronous reference frame

$I_s = \sqrt{i_{ds}^{e2} + i_{qs}^{e2}}$: stator current

$\lambda_{dr}, \lambda_{qr}$: rotor fluxes in stationary reference frame

$\lambda_{dr} = L_m I_d^e$: rotor flux

ω_e, ω_r : synchronous and mechanical frequency (*rad/s*).

$s = \omega_s / \omega_e$: slip

ω_s : slip frequency (rotor current frequency)

L_l , L_m: magnetizing and leakage inductance

R_s, R_r : stator, rotor resistance

T_e : electromagnetic torque ($N \cdot m$)

n_p : number of poles pairs

T: rotor temperature

^, *: estimated, reference values

The authors are with the Ohio State University, Columbus, Ohio.

I. Introduction

In high performance applications, the induction motor is controlled through field orientation techniques that require knowledge of the rotor speed. Since speed sensors decrease the reliability of a drive system (and increase its price), a common trend in motor control is to eliminate them and use a rotor speed observer to calculate the sought speed.

There are 4 major speed estimation techniques in literature:

open loop calculation (directly from motor equations), model reference adaptive (MRA) based, extended Kalman filter based, sliding mode observer based. All methods use the induction motor model to construct a flux-speed observer out of which speed information can be subtracted. MRA[7] observers for induction motors[2-4] define two models (usually stator and rotor) that yield the same output (flux, back-emf, reactive power etc). One model is speed independent while other model contains speed terms. The outputs of the two models are compared and their error is used to modify the value of the speed so that the error is driven to zero. An extended Kalman Filter method is proposed in [5] for the rotor speed identification. The idea consists in appending a fifth state (speed) to the motor equations and using an EKF to observe this fifth state. Although the method is innovative, it still suffers from parameter uncertainties and low speed estimation.

Common problems observed in all methods are: low speed estimation, speed estimation during fast transients, lack of robustness to parameter uncertainties. All known speed estimators depend on the induction motor model. Accurate knowledge of the model parameter is critical for speed estimation especially in the low speed range.

The goal of this research is the development of a sensorless torque control system for hybrid electric applications. Due to the dependency of the control system to parameter knowledge, modeling and parameter estimation over a wide range of operating conditions of induction motors is also developed.

II. HEV requirements for Sensorless Operation

A Hybrid Electric Vehicle (HEV) is an automobile in which the propulsion comprises both an Internal Combustion Engine (ICE) and an Electric Motor (EM). The most common type of HEV is the parallel type, in which the both ICE and EM are directly connected to the wheels. This structure presents a relative advantage in control over other induction motor applications, such as servos. The advantage is that the induction motor will virtually operate only at speeds above the idle speed of the IC engine (currently 300-600 rpm). The only situation in which the IM will need to operate at lower speed will be the transient from zero (stalled) to idle speed. This creates ground for the use of sensorless control techniques known to perform well except for low speed operation. However, all known speed sensorless techniques are sensitive to variation of parameters. The induction motor parameters vary with the operating conditions, as is the case with all electric motors. Furthermore, for a propulsion application the operating conditions will vary continuously. Speed (and input frequency) will change with driving cycles, traffic conditions etc. Temperature is influenced by loading but also by ambient, season etc. Operating flux levels although under closed loop control (unlike the other factors) will change with loading demands in order to obtain maximum energy efficiency. The parameters of the induction

motor model will change as the motor changes operating conditions, and these changes need to be accounted for in control.

III. Development Of Variable Frequency Models

Fig. 1 shows the induction motor model used in this research in stationary reference frame for q-axis (d-axis are similar). As noted in [15], the model is identical (without any loss of information) to the more common T – model in which the leakage inductance is separated in stator and rotor leakage.

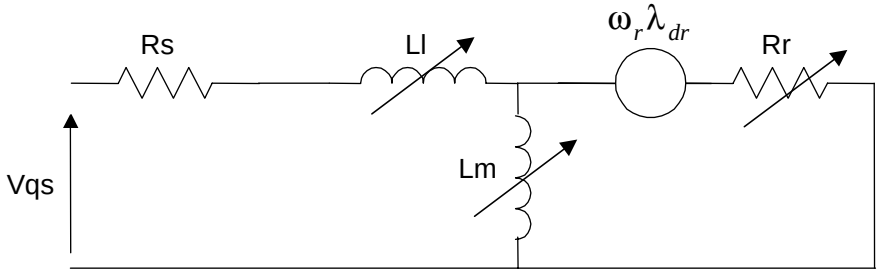

Fig. 1 Induction motor model in stationary reference frame(q-axis)

The following basic equations of induction machine can be derived:

$$\frac{d\lambda_{qr}}{dt} = n_p \omega_r \lambda_{dr} - \eta \lambda_{qr} + \eta L_m i_{qr} \tag{1}$$

$$\frac{d\lambda_{dr}}{dt} = -n_p \omega_r \lambda_{qr} - \eta \lambda_{dr} + \eta L_m i_{dr} \tag{2}$$

$$\frac{di_{qs}}{dt} = -\beta n_p \omega_r \lambda_{dr} + \eta\beta \lambda_{qr} - \gamma i_{qs} + \frac{1}{\sigma L_s} v_{qs} \tag{3}$$

$$\frac{di_{ds}}{dt} = \beta n_p \omega_r \lambda_{qr} + \eta\beta \lambda_{dr} - \gamma i_{ds} + \frac{1}{\sigma L_s} v_{ds} \tag{4}$$

with constants defined as follows :

$$\eta \equiv \frac{R_r}{L_m}, \sigma \equiv 1 - \frac{L_m}{L_l + L_m}, \beta \equiv \frac{1}{L_l}, \gamma \equiv \frac{R_s + R_r}{L_l}, \mu \equiv \frac{n_p}{J}$$

The electromagnetic torque expressed in terms of the state variables is:

$$T_e = \mu J \left(\lambda_{dr} i_{qs} - \lambda_{qr} i_{ds} \right) \tag{5}$$

The motor parameters were estimated off-line. The motor was run at various operating conditions and small disturbance tests were applied. The parameters were then estimated using a constrained optimization technique. Sensitivity analysis of the output to the parameters at different slip frequencies was employed to eliminate the parameters that yield low sensitivity. Table 1 shows the motor parameters at rated conditions:

Table 1 Induction Motor Rated Parameters

Rs	0.39 Ω
Ll	0.006 Henry
Lm	0.066 Henry
Rr	0.22 Ω

Outside rated conditions, the motor parameters change. Through a correlation analysis the authors isolated the parameter-operating condition dependency. A strong correlation was observed between L_m and i_{ds}^e. L_m clearly saturates with an increase in i_{ds}^e. A second order polynomial was used to represent the dependency.

$$L_m(i_{ds}^e) = k_1 \cdot {i_{ds}^e}^2 + k_2 \cdot i_{ds}^e + k_3 \quad (6)$$

Fig. 2 shows a comparison between the polynomial mapping and the results of the estimation.

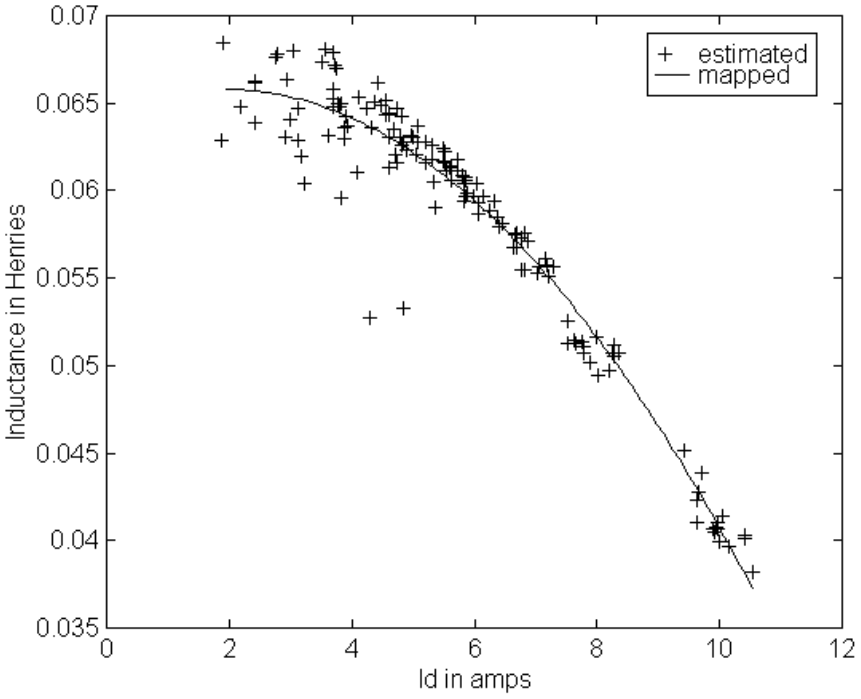

Fig. 2 Lm as function of i^e_{ds}

A strong correlation was also observed between L_l and *Is*. L_l saturates with an increase in *Is*. A linear approximation was used to represent the dependency.

$$L_l(I_s) = k_4 \cdot I_s + k_5 \quad (7)$$

Fig. 3 shows a comparison between the polynomial and the results of the estimation.

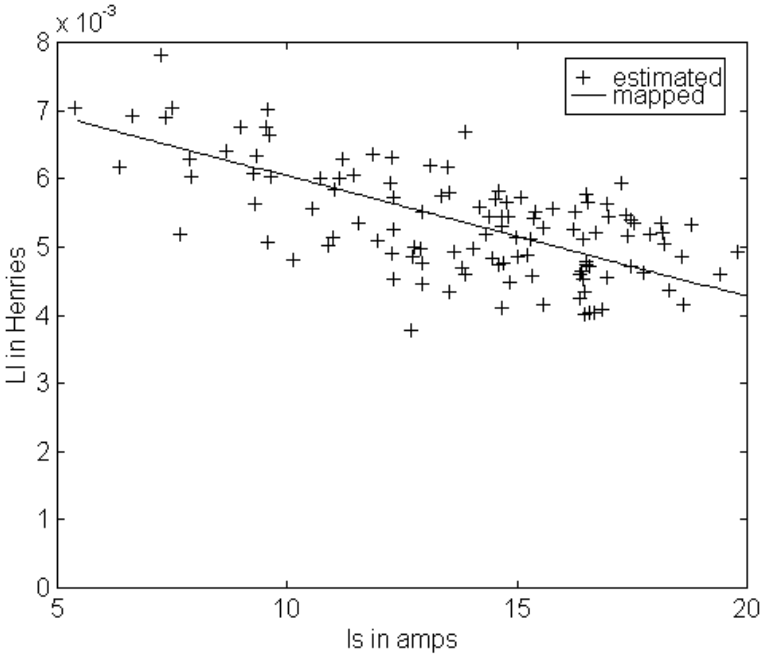

Fig. 3 L_l as function of Is

The rotor resistance varies as a function of two factors: slip frequency (through skin effect) and rotor temperature. Rotor temperature is hardly measurable and slip frequency is not available in a sensorless system. However, i^e_{qs} is correlated with both variables (temperature and slip frequency). i^e_{qs} is a measure of loading (e.g. temperature at constant flux) and slip frequency is proportional to i^e_{qs}. The correlation R_r and i^e_{qs} was measured experimentally and is shown in Fig.4.

$$R_r(i^e_{qs}) = k_6 \cdot i^e_{qs} + k_7 \tag{8}$$

A sudden variation in i^e_{qs} would not determine a sudden change in temperature since temperature does not change as fast. It could then be inferred that the $Rr(i^e_{qs})$ dependency is prone to errors for fast i^e_{qs} transients since although the $R_r(\omega_s)$ correlation still holds through i^e_{qs}, the

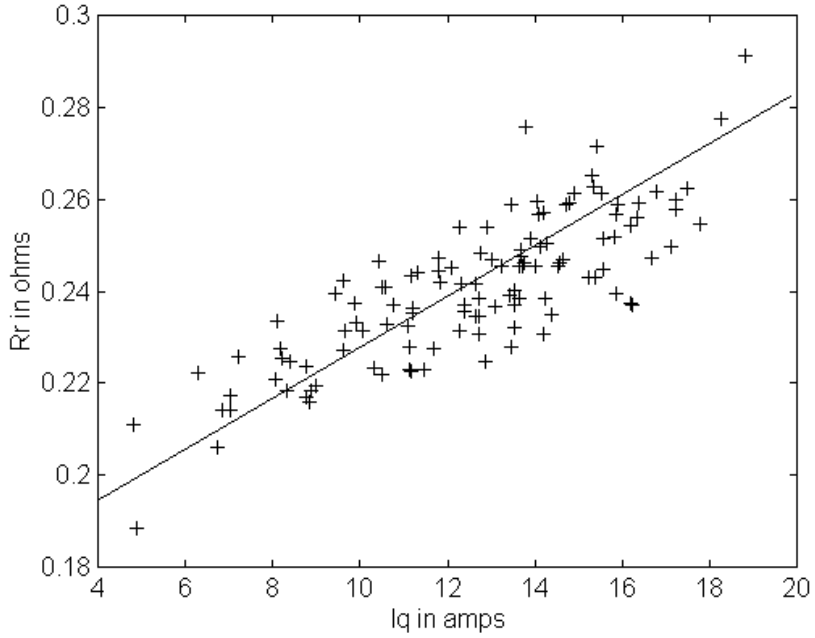

Fig. 4 Rr as function of i^e_{qs}

Rr(T) correlation is corrupted. However, the authors have observed that little error was introduced by using $Rr(i^e_{qs})$. Although the stator resistance varies with temperature, its variation did not seem to influence much the speed observation or the torque control. Also, due to the unavailability of a temperature sensor in the stator windings, it was considered at its rated value.

IV. Experimental setup

The experimental setup used in this research is shown in Fig. 5.

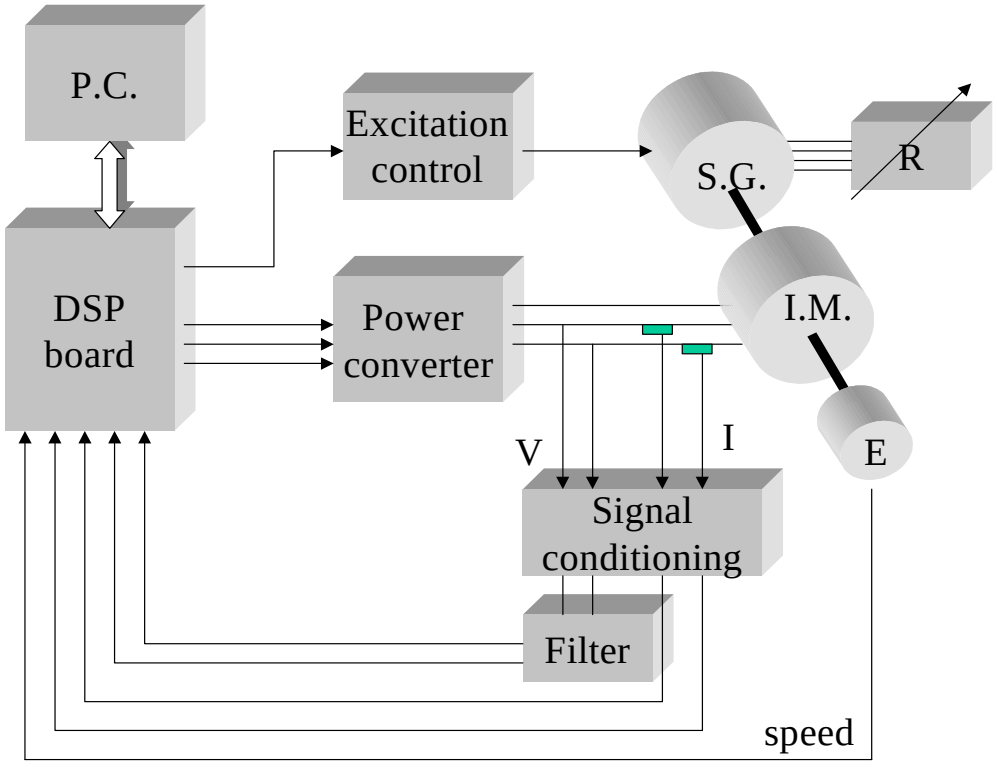

Fig. 5 Experimental setup

The induction motor (I.M.) is 3 phase, 4 pole, 5Hp, 1750 rpm 220 V squirrel cage. The synchronous generator (S.G.) is 2 phase, 2 pole, 5 Hp 440 V and is used as a load. The 5 kW variable resistor box (R) loads the synchronous generator. A variable DC power supply controls the excitation of the synchronous generator. The motor is driven by a 400V/30 A power converter capable of switching at 20 kHz. A dual processor (TMS320C31 Master and TMS320P14 Slave) DSP board used both for control and data acquisition. A 1024 pulse/revolution incremental optical encoder is used for speed measurement. The PWM cycle is 240 μs and the data acquisition sampling time is 60 μs. In order to avoid aliasing, the measured voltage is passed through a low pass filter prior to being acquired. The synchronous generator can be controlled simultaneously with the motor using the DSP board through the excitation voltage.

V. SENSORLESS TORQUE CONTROL DEVELOPMENT

A simplified block diagram of the control diagram is shown in Fig.6.

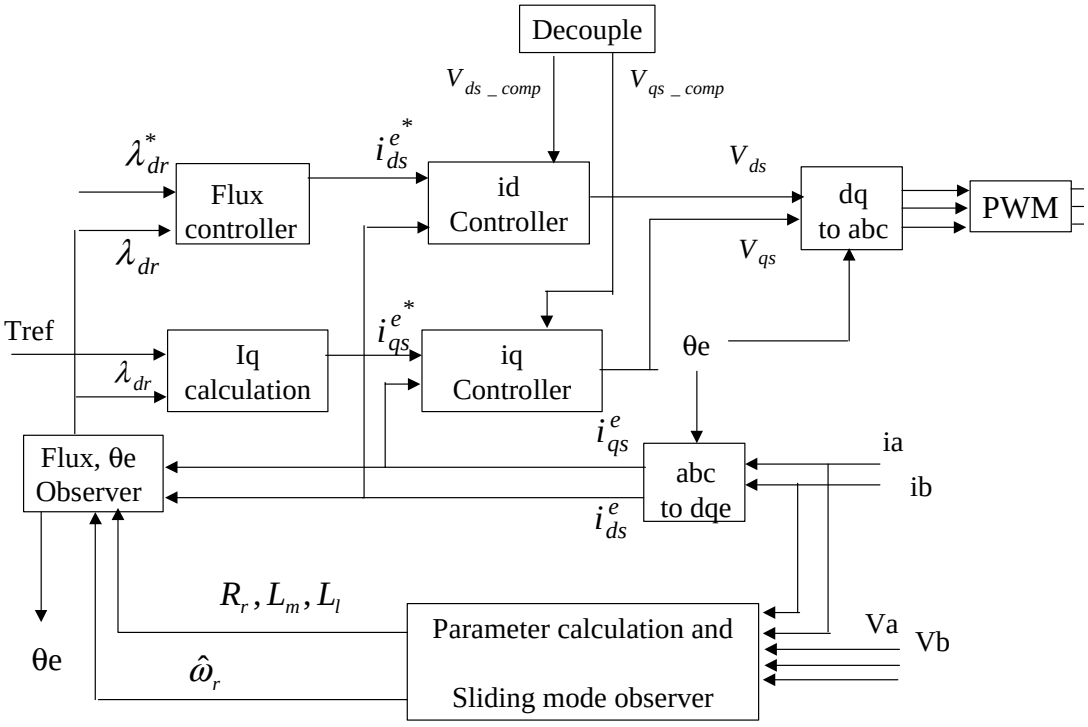

Fig. 6 Control structure

A. Adaptive sliding mode observer

The sliding mode observer equations are based on the induction motor current and flux equations:

$$\frac{d\hat{i}_{qs}}{dt} = -\beta\hat{\omega}_r\hat{\lambda}_{dr} + \eta\beta\hat{\lambda}_{qr} - \gamma\hat{i}_{qs} + \frac{1}{\sigma L_s}v_{qs} \tag{8}$$

$$\frac{d\hat{i}_{ds}}{dt} = \beta\hat{\omega}_r\hat{\lambda}_{qr} + \eta\beta\hat{\lambda}_{dr} - \gamma\hat{i}_{ds} + \frac{1}{\sigma L_s}v_{ds} \tag{9}$$

$$\frac{d\hat{\lambda}_{qr}}{dt} = \hat{\omega}_r\hat{\lambda}_{dr} - \eta\hat{\lambda}_{qr} + \eta L_m\hat{i}_{qs} \tag{10}$$

$$\frac{d\hat{\lambda}_{dr}}{dt} = -\hat{\omega}_r\hat{\lambda}_{qr} - \eta\hat{\lambda}_{dr} + \eta L_m\hat{i}_{ds} \tag{11}$$

Define a sliding surface as:

$$s = (\hat{i}_q - i_q)\hat{\lambda}_d - (\hat{i}_d - i_d)\hat{\lambda}_q \tag{12}$$

It can be analytically proven [8] that by selecting a speed estimate in the form of:

$$\hat{\omega} = \omega_0 sign(s) \tag{13}$$

with a large enough gain (ω_0) the sliding surface can be driven to zero in finite time. Since $\hat{\omega}$ is a switching function, a low pass filter is employed to extract the speed information (referred to as equivalent speed).

$$\hat{\omega}_{eq} = \frac{1}{1+s\cdot\tau}\hat{\omega} \quad (14)$$

The selection of the speed gain (ω_0) has two major constraints: the gain has to be large enough to insure that sliding mode can be enforced; a very large gain can yield to instability of the observer to discrete time integration. The authors used a linear function to tune the gain of the sliding mode observer to the filtered equivalent speed:

$$\omega_0 = \hat{\omega}_{\text{eq}} \cdot 0.3 + 60 \quad (15)$$

The presence of offsets in the measured signals can negatively influence the speed estimation. A DC offset in the measured input voltage "sees" only small impedance (just like in a dc test) and yields a large estimated current error. This in turn yields an oscillation in the estimated speed. In order to compensate the offsets, the authors used a recursive average value estimator for the measured voltages and currents.

$$\mathrm{V}_{offset}(k+1) = V_{measured}(k)\cdot\frac{1}{N} + \mathrm{V}_{offset}(k)\cdot\frac{N-1}{N} \quad (16)$$

where N is the number of samples for averaging and should be larger than the number of samples for one period at lowest input frequency. Since at steady state the signals are sinusoidal, the mean average is equal to the measurement offset and must be subtracted from the measurements prior to using into the observer.

The sliding mode observer structure is similar to a Luenberg observer in which the correcting linear factor is replaced by a sliding mode controller. This structure allows for the simultaneous observation of rotor fluxes. However, due to the limited sampling frequency, the numerical integration of the fourth order observer equations yields errors on flux observation, although the observer produces correct speed estimates. The integration error increases with supply frequency. Instead of using the flux-speed estimator for flux estimates, the authors used a second order observer:

$$\frac{d\hat{\lambda}_{qr}}{dt} = \hat{\omega}_r\hat{\lambda}_{dr} - \eta\hat{\lambda}_{qr} + \eta L_m i_{qs} \quad (17)$$

$$\frac{d\hat{\lambda}_{dr}}{dt} = -\hat{\omega}_r\hat{\lambda}_{qr} - \eta\hat{\lambda}_{dr} + \eta L_m i_{ds} \quad (18)$$

This observer produces correct flux estimates.

B. Alternative speed estimation for speed below 20 rpm

The sliding mode observer with parameters mapped to the operating conditions can not correctly estimate speeds below 20 rpm (in simulation the estimator works down to approximately 1 rpm). There are two main causes to this problem. First, the speed component in the observer equations becomes very small compared to the other terms in the equations. Second, in order to maintain a flux level below saturation, at low frequency the amplitude of supply voltage is very small (below 5 volts for speed below 20 rpm). Since voltage transducers are designed for approximately 100 times this value, there is considerable amount of noise and measurement error. The authors used instead of the sliding mode speed observer an input frequency observer. The observer is based on a least square estimator. Let two samples of the d-q axis currents at instant k be:

$$I_{ds}(k) = I\sin(\omega t + \varphi) \quad (19)$$

$$I_{qs}(k) = I\cos(\omega t + \varphi) \tag{20}$$

Assuming that the input frequency does not change considerably over the estimation process (approximately 5 ms), the *Ids* current can be written as:

$$y_k = h_k \cdot \theta_k \tag{21}$$

where $y_k = I_{ds}(k+1)$, $h_k = [I_{ds}(\mathrm{k}) \;\; I_{qs}(\mathrm{k})]$,

$\theta_k = [\cos(\omega TS) \;\; \sin(\omega TS)]$ and TS is the sampling time. The estimation process recursively calculates the parameter vector θ_k over 500 samples. The procedure can be summarized as:

1. Initialize $P_1^{-1} = h_1' \cdot h_1$ (22)

2. Recursively estimate θ_{n+1} using least squares:

$$P_n^{-1} = P_n^{-1} + h_n' \cdot h_n, \quad k_{w,n} = P_n \cdot h_n' \tag{23}$$

$$\theta_{n+1} = \theta_n + k_{w,n} \cdot (y_n - h_n \cdot \theta_n) \tag{24}$$

3. After 500 samples, calculate:

$$\omega = \frac{1}{TS}\sin^{-1}\left(\frac{\theta_n(2)}{\sqrt{\theta_n^2(2) + \theta_n^2(1)}}\right) \tag{25}$$

The frequency of the output is continuously monitored. When it falls below 1 Hz, the output of the sliding mode observer is not used anymore, and instead the supply frequency is used. Although perfect field orientation can not be achieved (because slip frequency is neglected), the motor performed relatively well at very low speed (below 20 rpm).

C. Discrete time Flux control – outer loop

The rotor flux dynamics in synchronous reference frame are linear and only dependent on the d-current input. A discrete time controller is used. The flux controller equation is:

$$i_{ds}^e(n) = \frac{\lambda_{dr}^{e*} - a_\lambda^* \cdot i_{dr}^e(n)}{b_\lambda^*} \tag{26}$$

where $a_\lambda^* = e^{-\eta \cdot TS2}$, $b_\lambda^* = \frac{1\text{-}a_\lambda^*}{\eta} \cdot L_m$, *TS2* - sampling time of the flux controller.

The flux reference can either be left constant or modified to accomplish certain requirements (minimum current, maximum efficiency, field weakening). In this research, the flux reference was kept constant and was weakened for speeds above rated. For speeds above rated, it is necessary to weaken the flux so that the supply voltage limits are not exceeded. The q-current reference is calculated from the torque equation to provide fast torque tracking.

$$i_{qs}^{e*} = \frac{T_{ref}}{\mu \cdot J \cdot \lambda_{dr}^e} \tag{27}$$

D. Current control- Inner loop

By rewriting the discrete version of the current equations one obtains:

$$i_{qs}^e(n+1) = a^* i_{qs}^e(n) + b^* V_{qs\_comp}(n) + b^* V_{qs}^e(n) \tag{28}$$

$$i_{ds}^{e}(n+1) = a^{*} i_{ds}^{e}(n) + b^{*} V_{ds\_comp}(n) + b^{*} V_{ds}^{e}(n) \tag{29}$$

where $a^{*} = e^{-\gamma \cdot TS}$, $b^{*} = \dfrac{1\text{-}a^{*}}{\gamma \cdot \sigma \cdot L_s}$, TS - sampling time

$$v_{qs\_comp} = -n_p \omega_r \lambda_r^{e} - \sigma L_s \omega_e i_{ds}^{e} \tag{30}$$

$$v_{ds\_comp} = \sigma L_s (\omega_e i_{qs}^{e} + \eta \cdot \beta \cdot \lambda_r^{e}) \tag{31}$$

The control signals can than be calculated so that the currents reach their references in one sampling period.

$$V_{qs}^{e}(n) = \frac{i_{qs}^{e^{*}} - a^{*} \cdot i_{qs}^{e}(n)}{b^{*}} - V_{qs\_comp}(n) \tag{32}$$

$$V_{ds}^{e}(n) = \frac{i_{ds}^{e^{*}} - a^{*} \cdot i_{ds}^{e}(n)}{b^{*}} - V_{ds\_comp}(n) \tag{33}$$

Since the calculated value of the control may exceed the maximal possibilities of the converter (DC bus voltage), an equivalent control was used. For the d-axis the control is:

$$V_{ds\_eq}^{e}(n) = \begin{cases} V_{ds}^{e}(n), & \text{if} \quad V_{ds}^{e}(n) \le U_{\max} \\ U_{\max} \cdot \dfrac{V_{ds}^{e}(n)}{\left\| V_{ds}^{e}(n) \right\|}, & \text{if} \quad V_{ds}^{e}(n) > U_{\max} \end{cases} \tag{34}$$

The q-axis control is similar. The net advantage of such control is that it preserves the good dynamic performance of the continuous time sliding mode control while eliminating chattering. However, since the control does not have an error correcting term (like a PI controller has), any parameter mismatch, delay, quantization error etc. will result in a steady state tracking error. The authors added a small error integrating term to the control to correct the problem.

$$V_{ds\_new}^{e}(n) = V_{ds\_eq}^{e}(n) + k_i \cdot (i_{ds}^{e^{*}}(n) - i_{ds}^{e}(n)) + e_{old}(n) \tag{35}$$

$$e_{old}(n) = k_i [i_{ds}^{e^{*}}(n-1) - i_{ds}^{e}(n-1)] + e_{old}(n-1), \; e_{old}(1) = 0$$

VI. Simulations and Experimental Results

A. Simulations

The control scheme presented in the previous section was simulated using Simulink. For operation of the motor above 20 rpm, the control scheme performed very well. The following graphs show different simulation tests performed at various speeds. The bottom graph shows the torque reference tracking. The observed torque is calculated using an observer that uses speed measurements. It can be seen that good tracking can be obtained in the entire range (except below 20 rpm). Figs. 10,11 show tests performed at very low speed (below 20 rpm). It can be observed that in the regions where speed fell below the threshold, speed estimates are constant for larger periods of time. This is due to the intrinsic delay of the least-square observer. Also, some oscillation can be seen around 20 rpm as the controller moves between sliding mode and least-square estimation of speed.

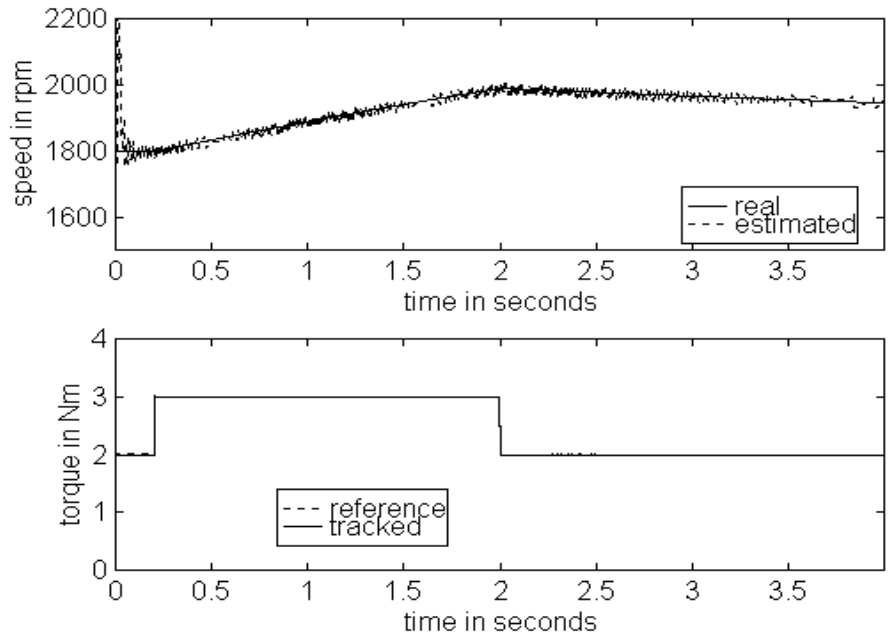

Fig. 7 Torque tracking in the 1500-2400 rpm range

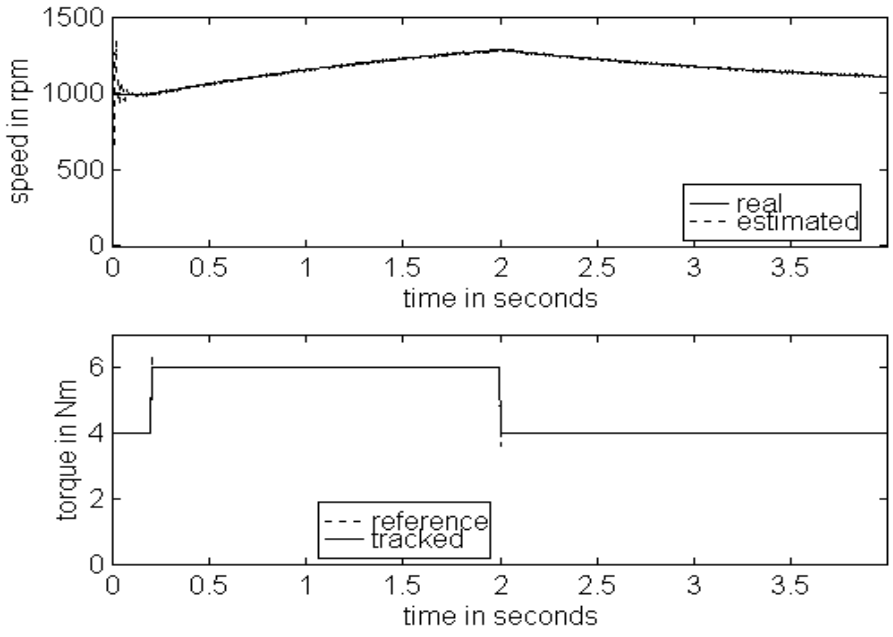

Fig. 8 Torque tracking in the 500-1500 rpm range

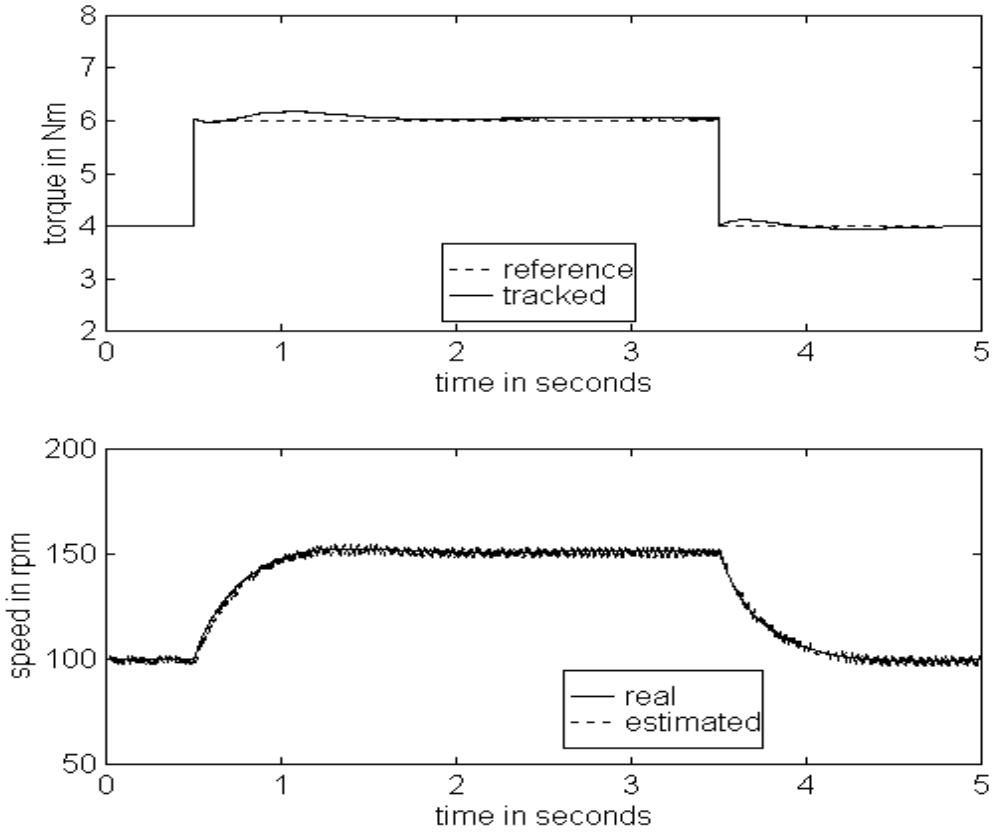

Fig. 9 Torque tracking in the 20-500 rpm range

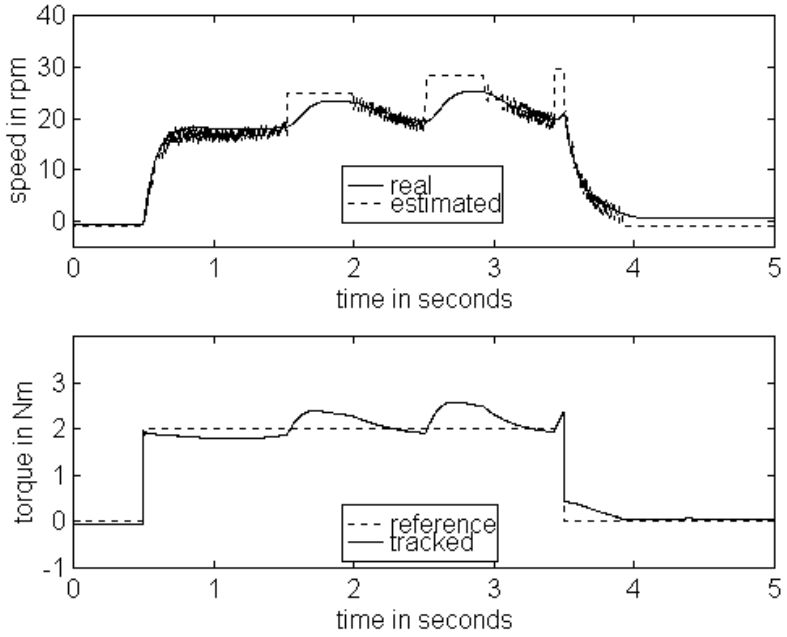

Fig. 10 Simulated torque and speed in the 0- 20 rpm range (example 1)

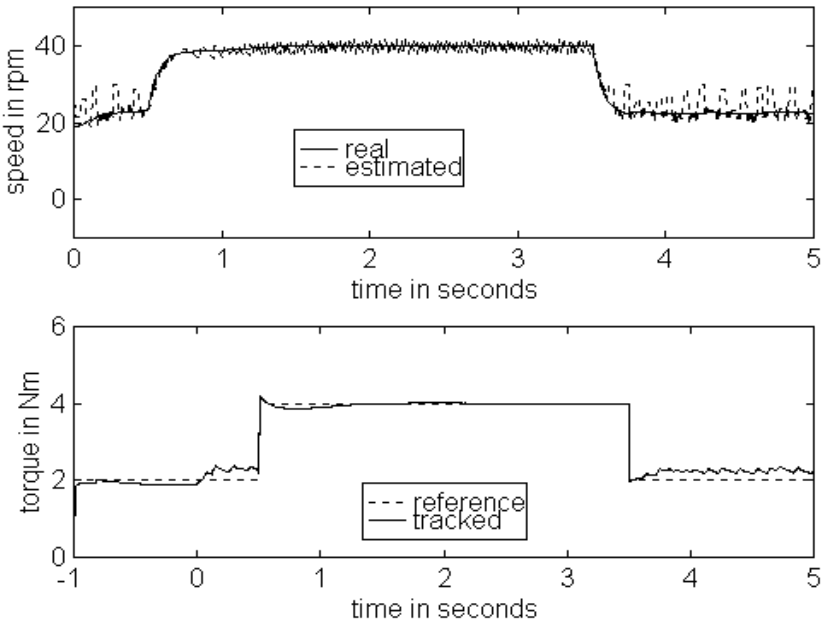

Fig. 11 Simulated torque and speed in the 0- 20 rpm range (example 2)

B. Experimental Results

1) Influence of parameter variation on speed estimation

The authors tested the sliding mode speed observer using rated parameters and varying (model-based) parameters. The flux and load levels were varied within their bounds. It was observed that except at rated conditions, the speed estimates for the model with rated (fixed) parameters exhibited considerable more error than for the model with varying parameters. Fig.12-15 present results of the tests. Fig. 16,17 presents the results together with the measured and observed speed for a low speed range test (20-50 rpm). In order to quantify the observer performance, the mean and the rms error between measured and estimated speed was recursively calculated. The estimation errors for all speed ranges (maximal values) are summarized in Table 2 for the model with constant parameters and in Table 3 for the proposed model. The mean, maximal and standard deviation of the error are calculated at steady state. All relative values are in respect to the measured speed. As reported for other speed estimators the relative value of the mean error decreases with a speed increase. While the relative mean error at speed above 1000 rpm is small for both models, considerable difference can be observed below this speed. For speed below 20 rpm, both models performed poorly, justifying the use of a non model-based speed estimator; its estimation errors are shown in Table 4.

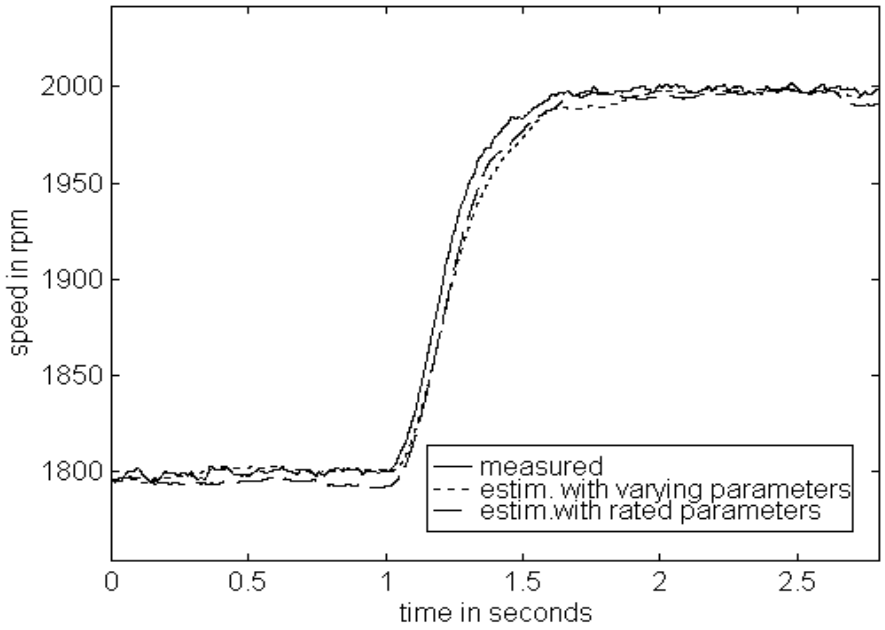

Fig. 12 Estimated speed in the 1500-2400 rpm range, with varying and rated parameters, medium flux, light load

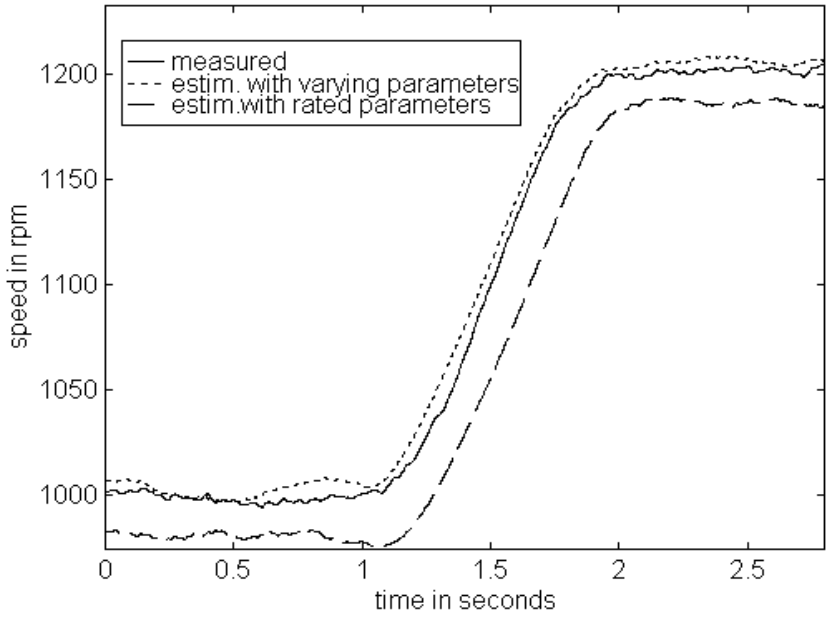

Fig. 13 Estimated speed in the 500-1500 rpm range with varying and rated parameters at low flux, medium load

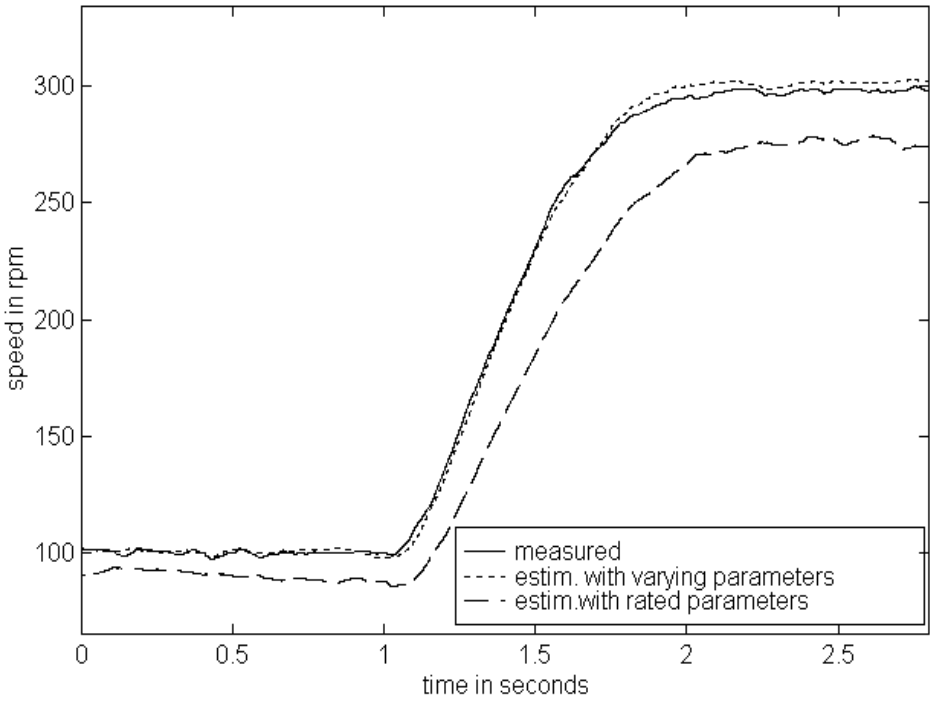

Fig. 14 Estimated speed in the 100-300 rpm range, with varying and rated parameters at low flux, high load

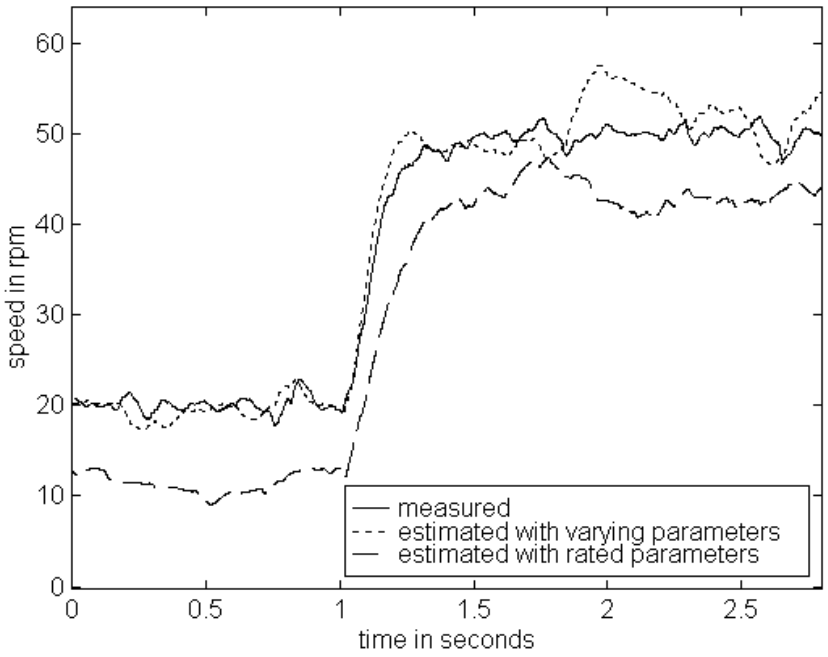

Fig. 15 Estimated speed in the 20-50 rpm range with varying and rated parameters at high flux, low load

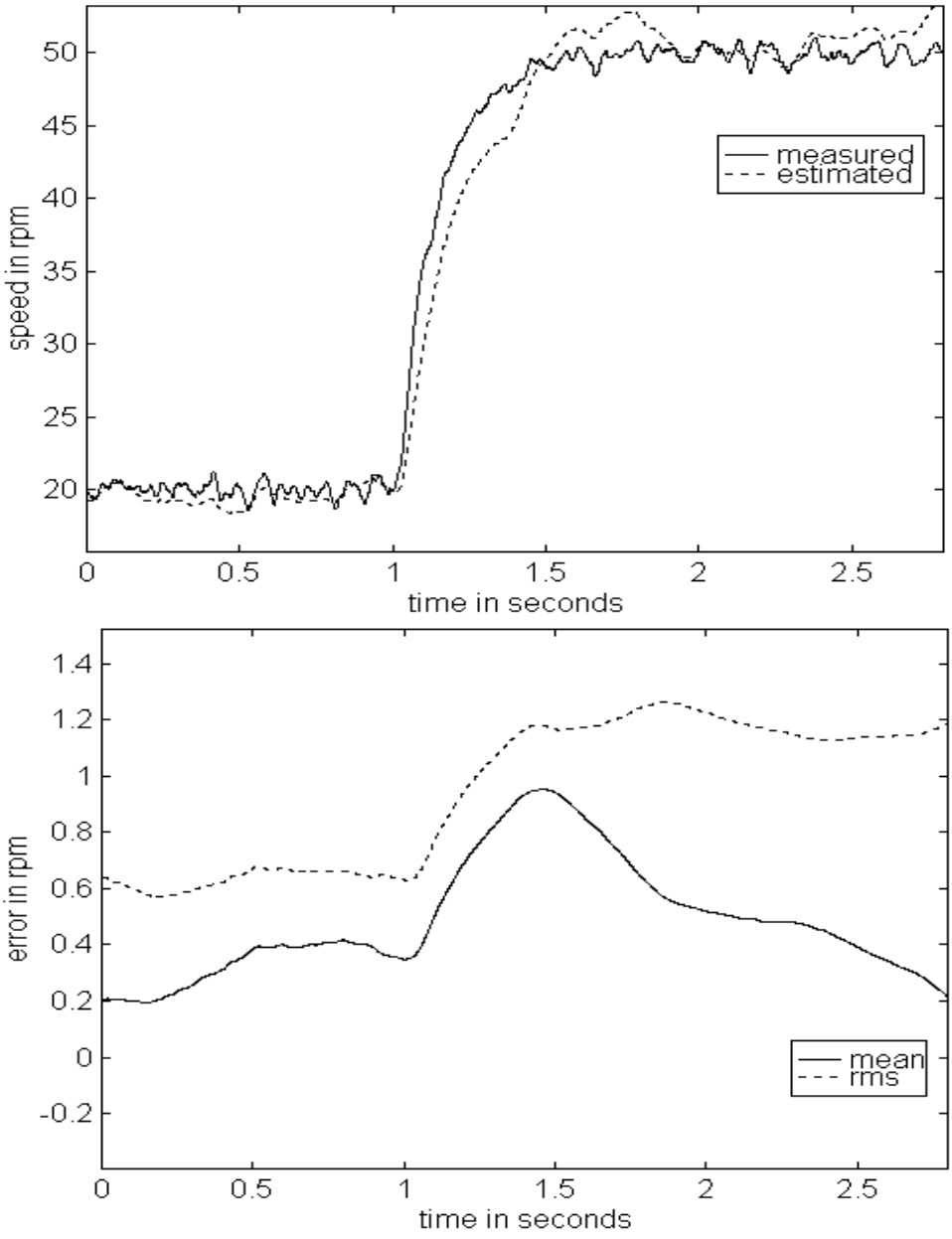

Fig. 16 Estimation errors in the 20-50 rpm range (example 1)

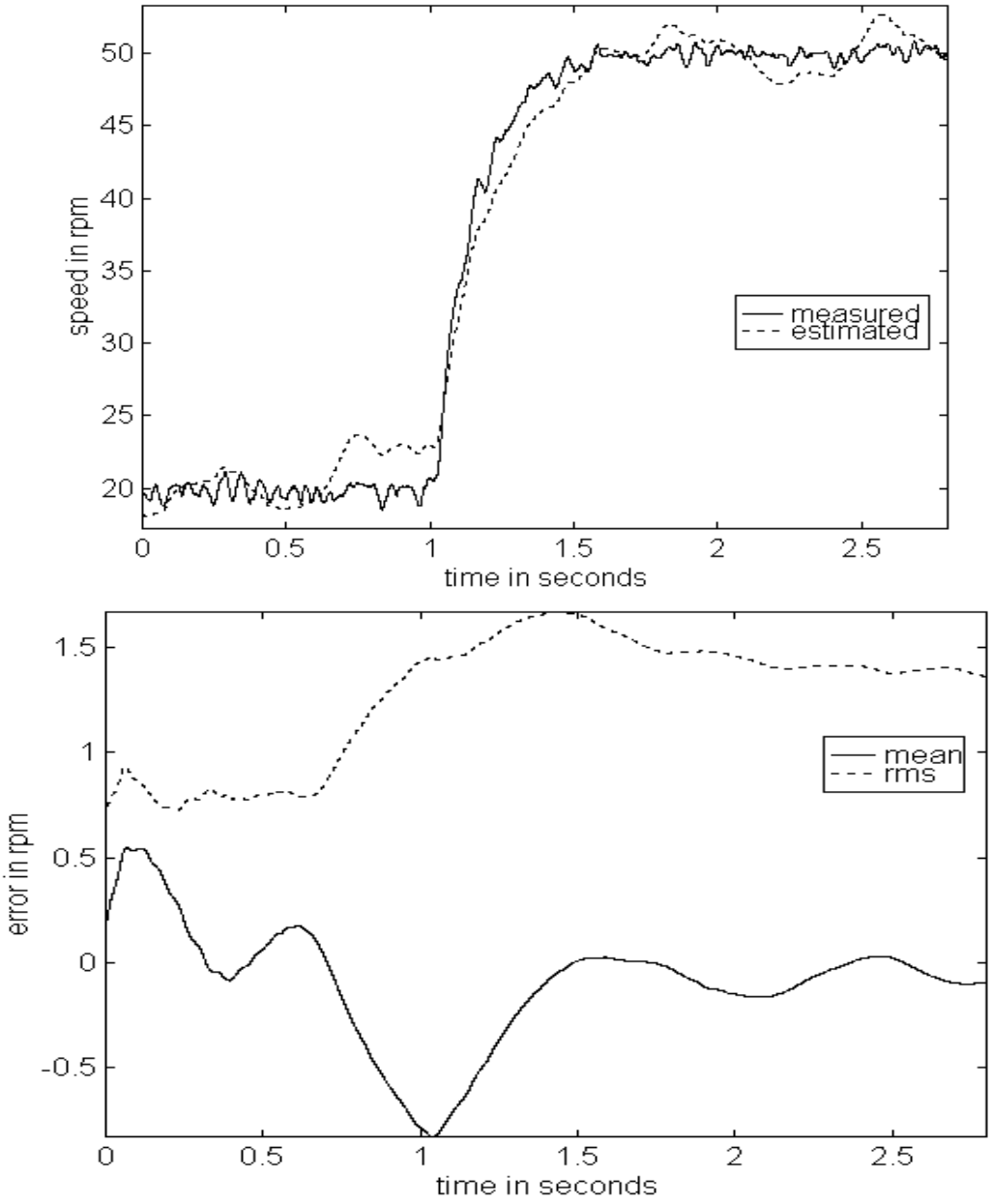

Fig. 17 Estimation errors in the 20-50 rpm range (example 2)

2) Control above 20 rpm

For operation of the motor above 20 rpm, the control scheme performed very well. Fig.18, 19 show different tests performed at various low speeds. The top graph shows the measured (dotted line) versus estimated speed (solid line).

Table 2 Estimation Error Characteristics for model with rated parameters

Speed	Mean Error		Standard deviation		Maximal Error	
(rpm)	Abs (rpm)	Relative (%)	Abs (rpm)	Relative (%)	Abs (rpm)	Relative (%)
20	7.73	38.63	3.19	15.97	10.27	51.34
50	6.90	13.80	2.18	4.35	9.31	18.61
100	9.52	9.52	1.45	1.45	12.60	12.60
200	25.57	12.79	7.99	4.00	39.37	19.68
500	21.50	4.30	6.81	1.36	33.63	6.73
1000	20.23	2.02	6.52	0.65	29.01	2.90
1200	16.96	1.41	1.80	0.15	19.72	1.64
1800	7.89	0.44	3.25	0.18	17.21	0.96
2000	11.76	0.59	3.64	0.18	18.45	0.92
2400	11.92	0.50	3.71	0.15	17.45	0.73

Table 3 Estimation Error Characteristics for proposed model

Speed	Mean Error		Standard deviation		Maximal Error	
(rpm)	Abs (rpm)	Relative (%)	Abs (rpm)	Relative (%)	Abs (rpm)	Relative (%)
20	2.36	11.78	2.69	13.47	6.03	30.14
50	4.03	8.07	2.27	4.55	6.11	12.22
100	8.23	8.23	3.26	3.26	13.75	13.75
200	7.16	3.58	5.96	2.98	13.44	6.72
500	6.82	1.36	4.42	0.88	12.50	2.50
1000	6.53	0.65	3.40	0.34	15.03	1.50
1200	8.15	0.68	2.62	0.22	10.66	0.89
1800	7.73	0.43	3.62	0.20	18.32	1.02
2000	9.70	0.48	3.71	0.19	19.10	0.96
2400	10.20	0.43	4.51	0.19	21.32	0.89

Table 4 Estimation Error Characteristics for least-square estimator

Speed	Mean Error		Standard deviation		Maximal Error	
(rpm)	Abs (rpm)	Relative (%)	Abs (rpm)	Relative (%)	Abs (rpm)	Relative (%)
0.5	1.91	382.00	1.82	364.00	4.1	820.00
5	3.64	72.80	2.49	49.80	8.96	179.2

						0
10	3.24	32.40	1.38	13.80	3.97	39.70
15	3.14	20.93	1.01	6.73	4.78	31.87
20	3.88	19.40	1.72	8.60	6.71	33.55

The bottom graph shows the torque reference tracking. The observed torque is calculated using an observer that uses speed measurements. It can be seen that good tracking can be obtained in the entire range (except below 20 rpm).

3) Control below 20 rpm

To qualify the situations in which the speed falls below the 20 rpm limit and which can produce large speed estimation errors, the authors used the frequency of the supply voltage as a measurement of speed. The supply frequency is continuously monitored. When it falls below 1 Hz, the output of the sliding mode observer is not used anymore, and instead the supply frequency is used. Fig 20, 21 show examples of these tests (Fig 21 also shows the mean and rms estimation error). Although speed observation is relatively poor, the system can still track torque. Furthermore, the very low speed operation of the induction motor is relatively rare in propulsion system for automotive application so the overall performance of the motor-controller system will not be affected considerably.

VII. CONCLUSIONS

A sensorless torque control system for induction motors was developed in this research. The system allows for fast and precise torque tracking over a wide range of speed, from 20 rpm to 2400 rpm. Both the speed observer and the control scheme are model based. The authors modeled the induction motor over a wide range of operating conditions, consisting of wide speed, load and flux ranges. By employing a sensitivity analysis of the output to each variable at various slip frequencies, the parameters that yielded low sensitivity were eliminated. Through a correlation study the dependencies between parameters and the variables characterizing operating conditions were isolated. The parameters were then mapped to these variables. The speed estimator is an adaptive sliding mode observer.

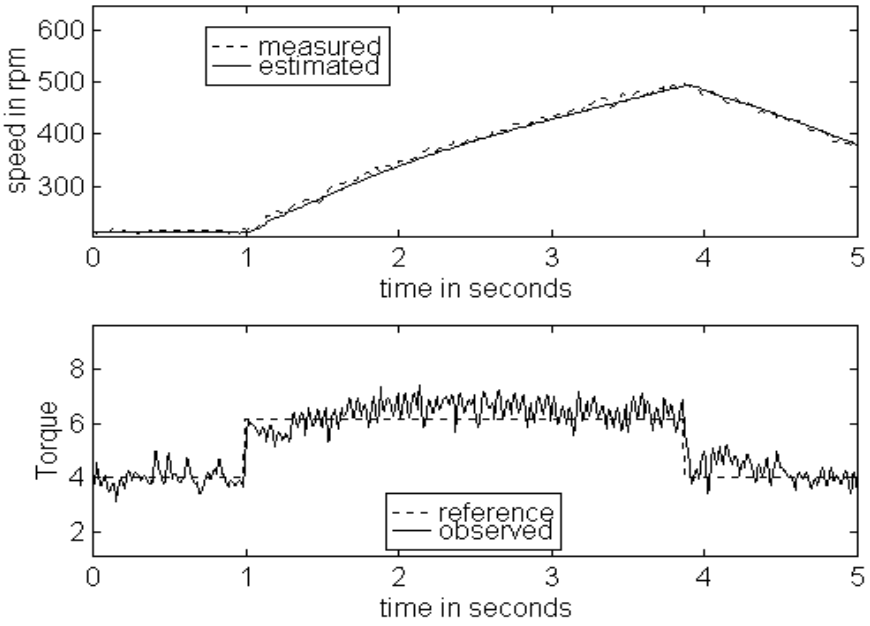

Fig. 18 Torque tracking in the 20-500 rpm range

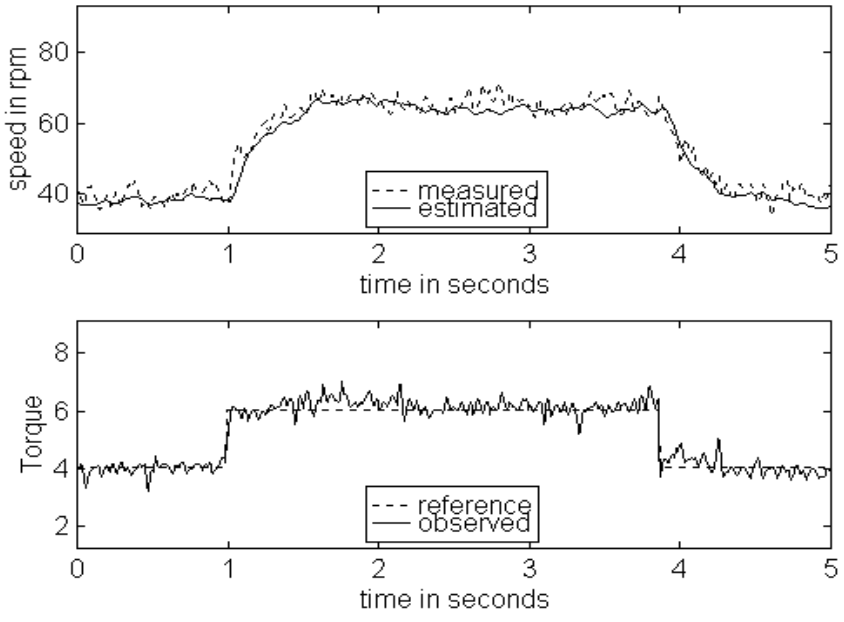

Fig. 19 Torque tracking in the 40-80 rpm range

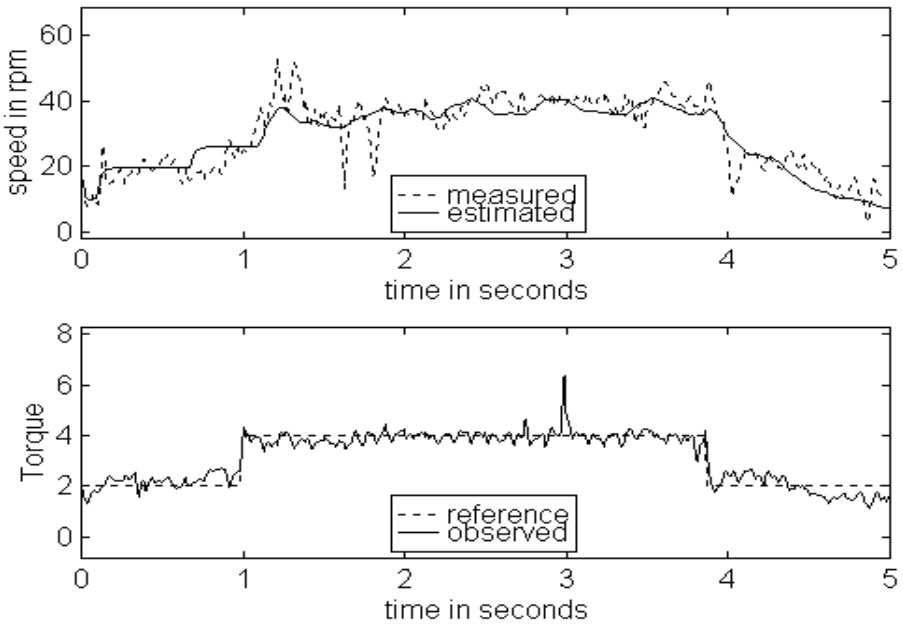

Fig. 20 Torque control in the 0- 50 rpm range (example 1)

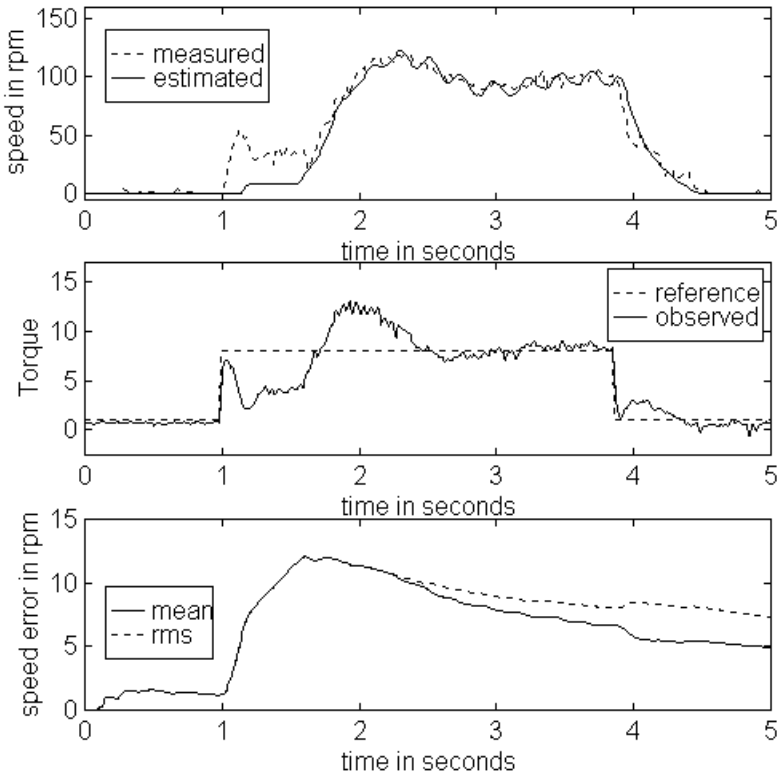

Fig. 21 Torque control in the 5- 100 rpm range (example 2)

This estimator performs better than MRA based estimators since no pure integration or differentiation of measured signals is needed. Gain adaptation of the observer is needed to stabilize the observer when integration errors are present. The design and implementation issues of the observer were analyzed (gain adaptation, offset cancellation etc). The observer can accurately observe speed down to approximately 20 rpm. Below this level, due to the low levels of voltage (1% of full scale) and to possible parameter mismatches the speed observations are inaccurate. The authors proposed an alternative method in which the input frequency is used as an observation of speed. The control algorithm is field oriented using discrete time sliding mode controllers for current and flux tracking. The discrete time sliding mode controller combines the fast response of any sliding mode controller while eliminating the chattering characteristic to continuos time sliding mode controllers. The controller was shown to perform very well except for the very low speed ranges. This poor performance at very low speed is due to the inaccurate speed observations at those speeds. However, the motor is able to respond with a speed increase when an increased torque command is received. Also, once the very low speed range is passed, the high performance control resumes. This low speed behavior is acceptable for HEV applications, when motor speed falls below stall speed (of IC engine) only at start-up and shut down.

The main problem with the proposed control scheme is the operation at very low speed. There is inaccurate speed estimation and the flux orientation is lost. Although the control performance is acceptable when torque control is sought, speed or position control would be impossible at that range, disqualifying this control strategy for servo applications.

VIII. REFERENCES

[1] Tsugutoshi Ohtani, "Vector Control of Induction Motor Without Shaft Encoder", *IEEE Trans. on Industry Applications,* Vol. 28 No.1, January/Febuary 1992

[2] Colin Schauder, "Adaptive Speed Identification for Vector Control of Induction Motors without Rotational Transducers", *IEEE Trans. On Industry Applications,* Vol. 28, No. 5, September 1992

[3] Fang-Zheng Peng, "Robust Identification for Speed-Sensorless Vector Control of Induction Motors", *IEEE Trans. On Industry Applications,* Vol. 30, No.5, September/October 1994

[4] Li Zhen, Longya Xu, "A Mutual MRAS Identification Scheme for Position Sensorless Field Orientation Control of Induction Machines", *IEEE IAS Annual Meeting,* pg. 159 - 165. 1995

[5] Young-Real Kim, Seung-Ki Sul, Min-Ho Park, "Speed Sensorless Vector Control of Induction Motor Using Extended Kalman Filter", *IEEE Trans. On Industry Applications,* Vol. 30, No.5, September/October 1994 pg. 1225-1233.

[6] P.L Jansen, R.D Lorenz, "Transducerless Position and Velocity Estimation in Induction and Salient AC Machines" *IEEE IAS Annual Meeting,* pg. 488 - 495. 1994

[7] Y.D Landau, Adaptive Control - The Model Reference Approach. New York : Marcel Dekker, 1979.

[8] V. Utkin, J. Guldner, J. Shi, *Sliding mode control in electromechanical systems,* Taylor & Francis, 1999

[9] L.A. de Souza Ribeiro, C.B. Jacobina, A.M. Nogueira Lima," Linear parameter estimation for induction machines considering the operating conditions ", *IEEE Transactions on Power Electronics* ,Vol. 14 , No. 1 , 1999 p. 62-73

[10] J. Stephan,M. Bodson,J. Chiasson, John ," Real-time estimation of the parameters and fluxes of induction motors", *IEEE Transactions on Industry Applications* ,Vol. 30 , No. 3 , 1994 p. 746-759

[11] X. Xu, D.W. Novotny," Implementation of direct stator flux orientation control on a versatile DSP based system ", *IEEE Transactions on Industry Applications* ,Vol. 27 , No. 4 , 1991 p. 694-700

[12] N. R. Klaes," Parameter identification of an induction machine with regard to dependencies on saturation ", *IEEE Transactions on Industry Applications* ,Vol. 29 , No. 6 , 1993 p. 1135-1140

[13] S.K. Sul, "A novel technique of rotor resistance estimation considering variation of mutual inductance", *IEEE Transactions on Industry Applications* ,Vol. 25 , No. 4 , 1989, p. 578-587

[14] T. Noguchi, S. Kondo, I. Takahashi, "Field-oriented control of an induction motor with robust on-line tuning of its parameters", *IEEE Transactions on Industry Applications*. v 33 n 1 Jan-Feb 1997. p 35-42.

[15] G.R. Slemon," Modelling of induction machines for electric drives ", *IEEE Transactions on Industry Applications*, Vol. 25 , No. 6 , 1989 p. 1126-1131

[16] R.T. Novotnak, J. Chiason, M. Bodson, "High performance motion control of induction motor with magnetic saturation", *IEEE Transaction on Control Systems Technology*, v.7, No.3, may 1999, pp.315-327

[17] B.K. Powell, K.E. Bailey, S. R. Cikanek, "Dynamic modeling and control of hybrid electric vehicle powertrain systems", *IEEE Control Systems Magazine*, v.18, No.5, 1998, pp. 17-33

[18] M. Ehsani, K.M. Rahman, H.A. Toliyat, "Propulsion system design of electric and hybrid vehicles", *IEEE Transactions on Industrial Electronics*, v.44, No.1, 1997, pp. 19-27

[19] K.M. Rahman, M. Ehsani, "Performance analysis of electric motor drives for electric and hybrid electric vehicle applications", *IEEE Workshop on Power Electronics in Transportation*, 1996, pp. 49-56